

# Trajectory of frequency stability in typical development

Joel Frohlich · Andrei Irimia · Shafali S. Jeste

Published online: 14 December 2014  
© Springer Science+Business Media New York 2014

**Abstract** This work explores a feature of brain dynamics, metastability, by which transients are observed in functional brain data. Metastability is a balance between static (stable) and dynamic (unstable) tendencies in electrophysiological brain activity. Furthermore, metastability is a theoretical mechanism underlying the rapid synchronization of cell assemblies that serve as neural substrates for cognitive states, and it has been associated with cognitive flexibility. While much previous research has sought to characterize metastability in the adult human brain, few studies have examined metastability in early development, in part because of the challenges of acquiring adequate, noise free continuous data in young children. To accomplish this endeavor, we studied a new method for characterizing the stability of EEG frequency in early childhood, as inspired by prior approaches for describing cortical phase resets in the scalp EEG of healthy adults. Specifically, we quantified the variance of the rate of change of the signal phase (i.e., frequency) as a proxy for phase resets (signal instability), given that phase resets occur almost simultaneously across large portions of the scalp. We tested our method in a cohort of 39 preschool age children (age =  $53 \pm 13.6$  months). We found that our outcome variable

of interest, frequency variance, was a promising marker of signal stability, as it increased with the number of phase resets in surrogate (artificial) signals. In our cohort of children, frequency variance decreased cross-sectionally with age ( $r = -0.47$ ,  $p = 0.0028$ ). EEG signal stability, as quantified by frequency variance, increases with age in preschool age children. Future studies will relate this biomarker with the development of executive function and cognitive flexibility in children, with the overarching goal of understanding metastability in atypical development.

**Keywords** Development · Metastability · Dynamics · Self-organized criticality · Electroencephalography · Biomarker

## Introduction

The electroencephalogram (EEG) signal recorded from scalp electrodes in humans can be understood in terms of state variables including amplitude, frequency, and topographic distribution. EEG state variables are known to be relatively static and dynamic at different temporal scales (Freeman and Kozma 2010; Freeman et al. 2003; Freeman 2004a, b; Kaplan et al. 2005; Thatcher et al. 2008, 2009a, b): this seemingly paradoxical balance between stability and instability is known as metastability. The prefix *meta-* generally modifies the stem of a word by raising it to a higher level of abstraction (Hofstadter 1979); for instance, *metadata* is data about data, and *metacognition* is cognition about cognition. Thus, metastability is the realization that the condition of stability is often unstable. An unresolved question in brain development is, how does the degree of this instability (i.e., the balance between stationarity and nonstationarity at different temporal scales) change with age and cortical

---

J. Frohlich (✉)  
Center for Autism Research and Treatment, University of California,  
Los Angeles, 760 Westwood Plaza, Semel Institute Suite 68-225, Los  
Angeles, CA 90095, USA  
e-mail: joelfrohlich@gmail.com

A. Irimia  
Institute for Neuroimaging and Informatics, Keck School of  
Medicine, University of Southern California, 2001 North Soto Street,  
SSB1-102, Los Angeles, CA 90032, USA

S. S. Jeste  
Center for Autism Research and Treatment, University of California,  
760 Westwood Plaza, Semel Institute Suite 68-237, Los Angeles,  
CA 90095, USA

maturation? Addressing this question in typical development is necessary to understand brain stability in relation to cognitive flexibility in neurodevelopmental disorders such as autism spectrum disorder (ASD). Furthermore, a greater balance between opposing stable and unstable inclinations in functional brain data implies greater brain complexity, a concept that, while variously defined (Coffey 1998; Janjarsjitt et al. 2008; Manor and Lipsitz 2012; Meyer-Lindenberg 1996; Sporns 2011; Tononi and Edelman 1998), has already shown potential as a biomarker of ASD (Bosl et al. 2011; Catarino et al. 2011; Eldridge et al. 2014; Ghanbari et al. 2013).

In dynamical systems theory, a metastable state is transiently stable until the system which exhibits it is perturbed to another—typically lower—energy state. This can be conceptualized as a ball stuck in a depression along the slope of a hill (Fig. 1): the ball remains at rest until a small perturbation dislodges it and it continues to the bottom of the hill. In neuroscience, the concept of metastability provides a theoretical foundation for explaining the observed coexistence of neural sensitivity to sensory input and robustness to intrinsic noise (Rabinovich et al. 2008) and, furthermore, it is the biophysical principle underlying the continuous emergence of new cell assemblies (Hebb 1949) through transient phase locking of neurons (Sporns 2011; Varela 1995; Werner 2007). Assuming that different cell assemblies are substrates for correspondingly different cognitive states (Varela 1995), metastability can be seen as a mechanism which endows the brain with cognitive flexibility by allowing it to shift between its seemingly opposing tendencies towards functional segregation and integration (Friston 1996, 2000; Werner 2007).

The duration of individual metastable epochs is challenging to directly measure, with most methods constrained by the need for long recordings of clean data. In studies of children, often limited by physiological artifact and variable compliance with testing, proxies of metastability are needed. Some examples include multiscale sample entropy (MSE, i.e., signal complexity) and dimensionality as estimated by principal component analysis (PCA) (Lippé et al. 2009; McIntosh et al. 2008). Another potential proxy of metastability not yet studied in early development is frequency variance. This measure can capture the synchronization and desynchronization of cell assemblies underlying cognitive states. Previous work by Freeman and colleagues has described large changes in instantaneous frequency (i.e., the time derivative of the analytic phase) of the resting-state EEG signal; these leaps, known as phase resets, are thought to represent transitions between metastable frequency states (Freeman and Holmes 2005; Freeman 2003, 2004a, b; Freeman et al. 2003, 2006). Importantly, the measurement

of frequency variance may not require clean data in every channel, as it can be examined on a channel by channel basis.

The objectives of our study were, firstly, to establish a method for measuring instantaneous frequency variance as a proxy for the phase resetting phenomenon described above and, secondly, to utilize this method to study cross-sectional development in a cohort of children of ages 2–6. Specifically, we applied this method to brain-related independent components (ICs) yielded from an independent component analysis (ICA) decomposition of resting-state EEG recordings from sensors in a modified 10–20 montage. The preschool age group was chosen for our cohort as it is the age at which large gains in executive function are achieved and the frontal lobes increase steadily in gray and white matter volumes (De Luca and Leventer 2010). Moreover, it is the age at which the clinical features of neurodevelopmental disorders such as ASD emerge (Cox et al. 1999; Fountain et al. 2011; Hertz-Picciotto and Delwiche 2009). We hypothesized that this method would serve as a proxy for artificial phase resets in surrogate signals and, in empirical signals, yield similar results when applied to minimal data (less than half a minute) and longer data (several minutes) from the same subjects, thus establishing it as a useful and valid method for pediatric populations. Furthermore, we hypothesized that frequency stability would decrease with age, reflecting faster synchronization and desynchronization of cell assemblies, the repertoire of which should expand with development. Finally, we believe that this method of quantifying frequency stability has possible advantages over methods that measure phase locking between EEG sensors (Thatcher et al. 2008, 2009a, b) and, thus, disregard the effective simultaneity of phase resets across large scalp distances (Freeman et al. 2003).

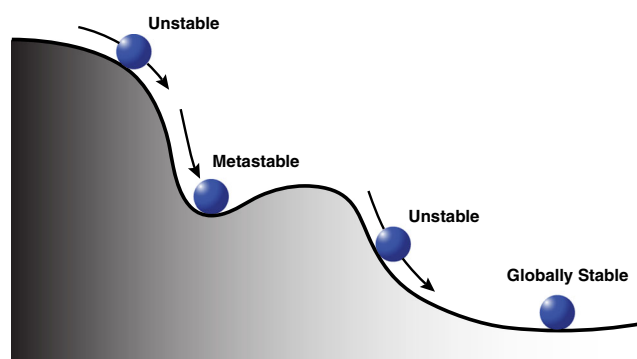


**Fig. 1** A metastable state is analogous to a ball caught in a depression along a hill: the state is transiently stable until perturbed to a lower energy state

## Methods

### Data collection and processing

Resting-state EEG signals were recorded using an array of 128 Ag/AgCl electrodes (Electrical Geodesics, Inc., Eugene, OR, USA) while children watched a video of bouncing soap bubbles. The Mullen Scales of Early Learning (MSEL) (Mullen 1995) or Differential Ability Scales Second Edition (DAS II) (Elliot 2007) were performed to verify that children had cognitive skills in the typical range. Children ages 2–6 ( $N=39$ , age= $53.0 \pm 13.6$  months, IQ= $118 \pm 14.2$ ) viewed abstract shapes on a computer monitor to capture attention for one session 120 s in duration. Recordings were amplified, digitized at a sampling rate of 250 Hz, and collected using Net Station (Electrical Geodesics, Inc., Eugene, OR, USA). Signals were bandpass filtered from 1 to 50 Hz and partitioned into 256 sample segments, in view of the fact that segments containing a number of data points equal to a power of 2 are ideal for use with the fast Fourier transform (FFT). Sensors which did not function properly either during individual recording segments or throughout the entire recording were marked as such using a 200  $\mu$ V threshold, and their signals were interpolated from neighboring channels. To limit the proportion of interpolated data, an upper limit was established such that the number of interpolated data points in a segment should not exceed the square root of the total number of data points. Accordingly, segments with more than 11 channels whose recordings needed to be inferred via interpolation were rejected on these grounds. Channels that were (A) only interpolated within a given segment and (B) interpolated for the entire recording both counted towards the 11 channel interpolation limit for a given segment. Preprocessed signals were exported to MATLAB and analyzed using the EEGLAB toolbox (Delorme and Makeig 2004), where they were visually inspected so that segments containing ocular or muscle artifacts could be rejected.

### Independent component analysis

Subsequent to signal preprocessing, a combined approach involving PCA followed by ICA was utilized to identify one or more brain-related ICs in the recordings. This was accomplished using the modified infomax ICA algorithm provided by the EEGLAB toolbox (Amari et al. 1996; Bell and Sejnowski 1995; Delorme and Makeig 2004; Lee et al. 1999). Recordings acquired using 20 sensors approximately corresponding to the international 10–20 montage were concatenated across subjects prior to PCA/ICA in order to ensure that (A) each subject had the same signal decomposition and that (B) subsequent analysis results would not be confounded by distinct ICA decompositions across subjects. Because recordings were vertex-referenced, sensors immediately anterior (FCz) and posterior (CPz) to Cz were substituted for Cz in this approximation of the 10–20 montage. Use of this montage serves as a spatial filter and

increases the ratio between the number of time points in each signal to the number of variables in each dataset, which is an important consideration for assessing the validity of PCA and ICA decompositions (Onton et al. 2006). We first performed a dimensionality reduction to 8 principal components (PCs), which were subsequently decomposed into 8 sub-Gaussian ICs.

### Frequency variance

As an inverse measure of frequency stability and as a proxy for the phase reset phenomenon, we examined the variance of the instantaneous frequencies exhibited by each IC during the resting-state. To investigate frequency metastability, we used the Hilbert transform, which is a linear transform similar to the Fourier transform but with higher temporal resolution and lower frequency resolution. This higher temporal resolution is necessary for estimating the instantaneous frequency of the signal. The Hilbert transform  $H(u)$  of some signal  $u(t)$  is given by the integral equation

$$H(u) = \frac{1}{\pi} \text{P.V.} \int_{-\infty}^{+\infty} u(t')/(t-t') dt' \quad (1)$$

where P.V. is the Cauchy principal value needed to solve the improper integral. The imaginary solution together with the real signal  $u(t)$  yields the analytic signal  $V(t)$  by the following relation:

$$V(t) = u(t) + iH(u) \quad (2)$$

From these real and imaginary components of the analytic signal, it is trivial to compute the analytic phase,  $\Phi(t)$ :

$$\Phi(t) = \text{atan2}[H(u), u(t)], \quad \Phi(t) \in [-\pi, +\pi] \quad (3)$$

For the purpose of taking the time derivative of  $\Phi(t)$ , it is necessary to unwrap the phase angles so that they are no longer bounded between  $-\pi$  and  $+\pi$ . This is accomplished by the unwrap function, which adds multiples of  $\pm 2\pi$  at temporal differences in  $\Phi(t)$  greater than a tolerance value of  $\pi$ . The instantaneous frequency,  $f(t)$ , is the time derivative of the unwrapped analytic phase of the signal:

$$\text{unwrap}[\Delta\Phi_i(t)] = \begin{cases} \Delta\Phi_i(t) + 2\pi, & \Delta\Phi_i(t) \leq -\pi \\ \Delta\Phi_i(t), & -\pi < \Delta\Phi_i(t) < \pi \\ \Delta\Phi_i(t) - 2\pi, & \Delta\Phi_i(t) \geq \pi \end{cases} \quad (4)$$

$$f(t) = \frac{d\text{unwrap}[\Phi(t)]}{dt} \quad (5)$$

One can imagine the analytic phase (i.e., the antiderivative of instantaneous frequency) of the EEG signal in the context

of turbulent ascent by a passenger jet into the air. Normally, the ascent is smooth and altitude is a monotonically increasing function of time. However, occasional turbulence causes large dips and jumps in the altitude of the jet. Such dips and jumps (analogous to phase resets, Fig. 2a) bracket periods of otherwise stable ascent velocity (analogous to frequency, Fig. 2b).

To emphasize local variance, a normalization operation was performed whereby the mean instantaneous frequency was subtracted from all instantaneous frequency values.

$$f_k = f_i(t) - N^{-1} \sum_{j=1}^N f_j(t) \quad (6)$$

The variance  $f_v$  of the normalized instantaneous frequency  $f_k$  can be conceptualized as a surrogate measure of phase reset, and the frequency stability  $f_s$  of the signal is defined as the inverse of  $f_v$ :

$$f_v = \text{var}(f_k) \quad (7)$$

$$f_s = 1/f_v \quad (8)$$

To ensure that  $f_v$  is a good proxy of phase resetting, we induced the latter in several surrogate signals of length  $N$  at random time points using amplitude inversion and measured  $f_v$  as a function of the number of phase resets  $n$ . Four types of surrogate signals were used: sinusoids, pink (power-law) noise, white noise, and the logistic map. The logistic map is a 2nd degree polynomial mapping that demonstrates chaotic behavior, or extreme sensitivity to initial conditions, for certain parameter values. Unlike colored noise, the logistic map mimics deterministic chaos in the EEG signal (Fell et al. 1993; Meyer-Lindenberg 1996; Soong and Stuart 1989; Stam 2005; Wang et al. 2010). It is expressed by the following recurrence relation:

$$x_{n+1} = rx_n(1-x_n) \quad (9)$$

Our logistic map surrogate signal used parameter values  $x_0=0.3$ ,  $r=3.7$ , a point in parameter space that yields chaotic solutions.

Unlike the logistic map, the complexity of colored noise signals is the result of a stochastic process. Pink noise signals are colored noise with power spectral density inversely proportional to the frequency of the signal raised to some power  $\alpha$ . For our surrogate signals, we used pink noise with  $\alpha=2$ . Pink noise surrogate EEG signals were generated using MATLAB code by Little et al. (2007), distributed for free online at <http://www.maxlittle.net/software/>.

Having measured  $f_v$  as a function of  $n$  in surrogate signals, we held  $n/N$  constant at 0.04, mimicking physiological resets

rates (Freeman et al. 2003) at a sampling rate of 250 Hz, and measured  $f_v(N)$  over 10 simulated trials to infer the minimum value of  $N$  for which  $f_v(N)$  assumes a relatively constant value in the limit of large  $N$ .

For empirical datasets, three separate analyses (Analysis 1-3) were performed using subjects' left-posterior IC signals. In each analysis, the IC signal was beta-gamma filtered from 12 to 48 Hz using inverse FFT filtering. Because ICA was used in conjunction with traditional methods of artifact reduction, any artifact which failed to be reduced using traditional methods of artifact reduction should have been reduced using ICA. The goal of Analysis 1 was to compute  $f_v$  while controlling for length of the signal  $N$ , as this variable threatens to confound measurements of variance if not adequately constrained. The first 29 segments of the IC signal were examined, with 29 corresponding to the number of artifact-free segments in the dataset of shortest time length. Linear trends were removed from all 29 segments to eliminate spurious phase resets possibly created by concatenating discontinuous segments. A single  $f_v$  value for the entire IC signal was then computed. Directional statistics (Philips 2009) were utilized to examine the directional variance  $S$  of signal phases in the IC, where  $S=0$  indicates absolute phase preference and  $S=1$  indicates zero phase preference.

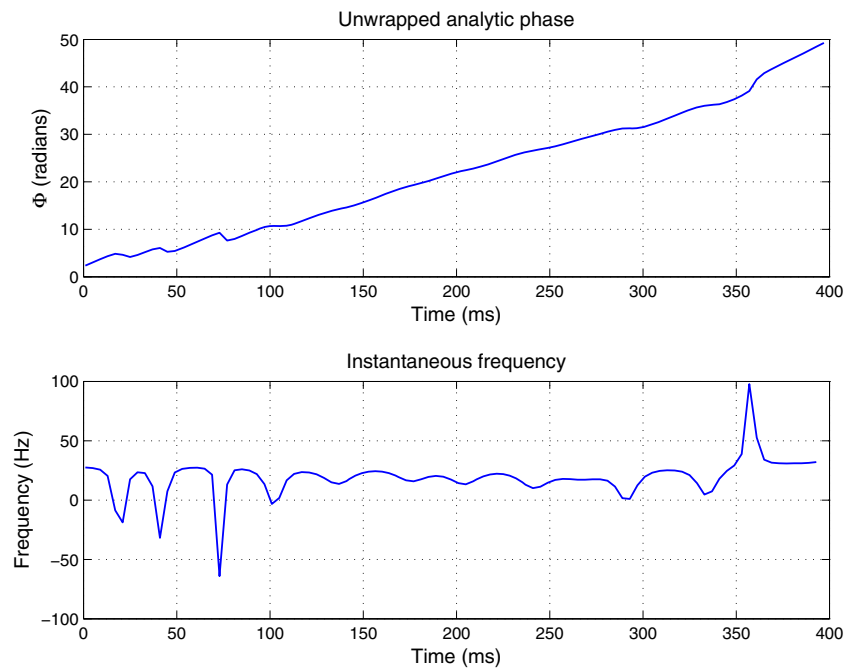
In Analysis 2, the length of the IC signal was not controlled for and all artifact-free segments were used. As with Analysis 1, signals from each subject's left-posterior IC were beta-gamma bandpass filtered and  $S$  was utilized as a measure of phase preference. Each signal segment was detrended and a single  $f_v$  value was computed for the entire signal.

In Analysis 3,  $f_v$  was computed for each artifact-free segment of the beta-gamma filtered left-posterior IC signal, and the mean intra-segment  $f_v$  value was adopted as a measure of frequency variance for each subject. Intra-segment phase preference was also measured using  $S$ . Because the possibility of spurious phase changes at discontinuities created by concatenation cannot be entirely eliminated even by detrending segments, this analysis was necessary to completely control for such artifactual phase changes. Furthermore, this analysis measures  $f_v$  without detrending EEG signal segments, eliminating the risk of variance reduction as a consequence.

To reiterate, our study examined frequency variance  $f_v$  in two contexts: (A) surrogate signals, for which the number of phase resets could be directly manipulated, and (B) brain-related ICs from resting-state EEG recordings of typically developing children with a scalp topography consistent with a left-posterior cortical source. For each empirical dataset, the IC of interest was isolated and the FFT was then used to filter recordings into the 12–48 Hz bandpass, chosen so as to include beta-gamma oscillations which are known to be carrier waves for phase resets in human scalp EEG (Freeman et al. 2003). After filtering, the Hilbert transform was applied and the distribution of instantaneous frequencies was computed for the subject. The variance  $f_v$  of this distribution was then investigated as a proxy



**Fig. 2** Unwrapping the analytic phase of a bandpass-filtered EEG signal yields an almost monotonically increasing ramp function (a). Small discontinuities in the otherwise smooth ramp are phase resets. The time derivative of the unwrapped analytic phase is the instantaneous frequency of the signal (b). Instantaneous frequencies obtained from the analytic phase are instances of angular frequency and, as such, can assume negative values



for phase resetting. To ensure that  $f_v$  was not influenced by the number  $N$  of time points in the signal, three separate analyses were performed using each subject's IC of interest. Analysis 1 and Analysis 2 both measured  $f_v$  using concatenated, detrended EEG segments. However, Analysis 1 controlled for signal length  $N$ , allowing effects of  $N$  on  $f_v$  to be constrained and examined. Analysis 3 measured the mean intra-segment frequency variance. This controlled for discontinuities in the signal and eliminated the need for removing linear trends.

## Results

### Surrogate EEG signals

In surrogate signals, we found that, for sinusoids, pink noise (i.e., power law-distributed noise) with power law exponent  $\alpha=2$ , and a signal with deterministic chaos properties (logistic map,  $x_0=0.3$ ,  $r=3.7$ ) the curve  $f_v(n)$  increases monotonically with added noise (Fig. 3). The only signal for which  $f_v$  did not increase as a function of  $n$  was Gaussian white noise. Subsequently,  $f_v(N)$  was measured while holding  $n/N$  constant at 0.04 to ascertain the minimum length of data for which meaningful measurement of  $f_v$  can be made. We found that the  $f_v(N)$  curve follows the behavior of a damped, noisy oscillation when examined as a function of the independent variable  $N$  (Fig. 4). To find the value of  $N$  where the oscillation asymptotes, we examined the cumulative variance of  $f_v(N)$ , i.e., the variability of the instantaneous frequency variance, or “metavariance,” as a function of signal length. The metavariance monotonically

decreases following a power law and as a function of signal length after  $\sim 2 \times 10^3$  samples (Fig. 5).

### Resting-state EEG signals

Data from all subjects were concatenated for the decomposition, and thus all subjects shared precisely the same ICA weights matrix (Fig. 6). An IC which was most likely related to brain activity was identified in the decomposition of the concatenated data, corresponding to a dipolar pattern over the left posterior region of the head (Fig. 7). This IC was selected as the target of further analysis because (A) other ICs were related to eye-blinks or noise, (B) other ICs lacked a clear dipolar pattern (Fig. 6), and (C) the gamma amplitude of posterior parietal signals is thought to be modulated by thalamic alpha activity (Roux et al. 2013), which in turn is theoretically implicated in gamma band phase resetting (Freeman et al. 2003; Thatcher et al. 2009b). The remainder of our analysis is consequently focused exclusively on this IC whose topology resembles that of a left posterior dipole. Averaging the power spectral density (PSD) of this IC across subjects showed that posterior alpha rhythms occur at 8–9 Hz in our cohort of children (Fig. 8).

Using all clean EEG segments, we found a weak, yet not significant, correlation between  $f_v$  and signal length  $N$  ( $r=0.25$ ,  $p=0.12$ ). Additionally, because the phase preference of IC signals correlated with signal length  $N$  ( $r=0.53$ ,  $p=5.0 \times 10^{-4}$ ), we appropriately took the precaution described in the methods section of performing three separate analyses.

In Analysis 1, the first 29 segments ( $N=7.42 \times 10^3$ ) of artifact-free recordings from each subject were examined (this corresponded to the length of the shortest artifact-free dataset).

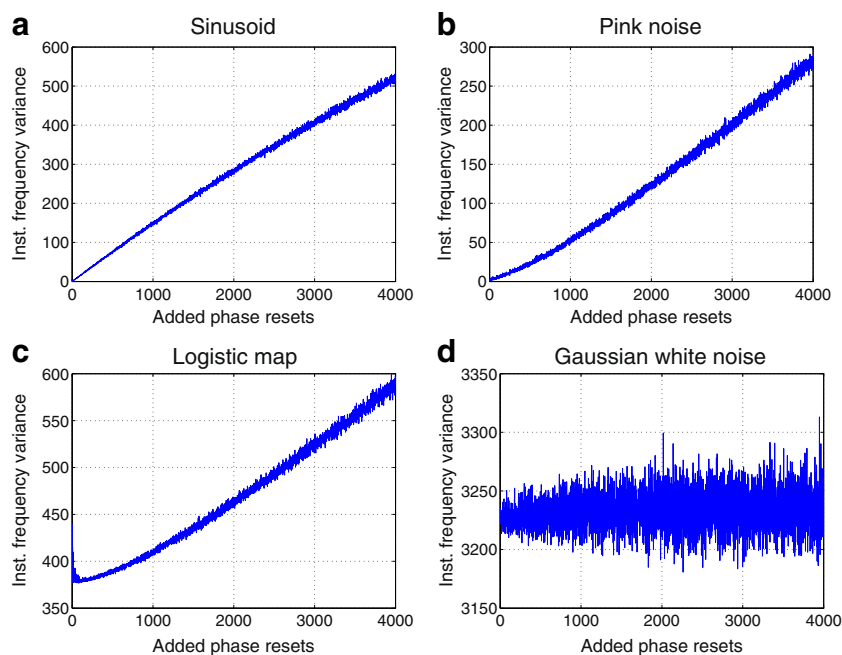


**Fig. 3** Four surrogate signals consisting of  $5 \times 10^4$  time points each were used to assess frequency variance as a proxy of phase resets. Shown are the profiles of the instantaneous frequency variance as a function of phase resets in the surrogate signal: **a** sinusoid, **b** pink (power law) noise with power law exponent  $\alpha=2$ , **c** signal exhibiting deterministic chaos generated using a one-dimensional logistic map ( $x_0=0.3$ ,  $r=3.7$ ), and **d**

Gaussian white noise with a signal mean of zero and unity variance. Phase resets were added to surrogate signals at random time points using the amplitude inversion method. As expected, frequency variance is seen to increase almost monotonically with the number of phase resets for all surrogate signals except in the case of Gaussian white noise

Using these IC segments, we found a significant negative correlation between age and  $f_v$  ( $r=-0.38$ ,  $p=0.018$ ; Fig. 9a). The IC of interest showed little to no phase preference as measured by directional variance ( $S=0.99 \pm 0.0046$ ).

Furthermore, there was no correlation between phase preference, as measured by  $S$ , and  $f_v$  ( $r=-0.13$ ,  $p=0.94$ ).

In Analysis 2, which used the entire IC signal composed of all artifact-free segments, we also found a significant negative correlation between age and  $f_v$  ( $r=-0.41$ ,  $p=0.010$ ; Fig. 9b). As with the first analysis, the IC signal showed no phase preference as measured by directional variance ( $S=0.99 \pm 0.0035$ ), nor did  $S$  correlate with  $f_v$  ( $r=0.020$ ,  $p=0.90$ ).

In Analysis 3—in which linear trends were not removed from segments and the mean intra-segment frequency variance was adopted as  $f_v$ —a negative correlation between age and  $f_v$  was found which was both significant and stronger than that discovered in the previous two analyses ( $r=-0.47$ ,  $p=0.0028$ ; Fig. 9c). Once again, no phase preference was found ( $S=0.96 \pm 0.0023$ ), and  $S$  showed no correlation with  $f_v$  ( $r=0.022$ ,  $p=0.89$ ).

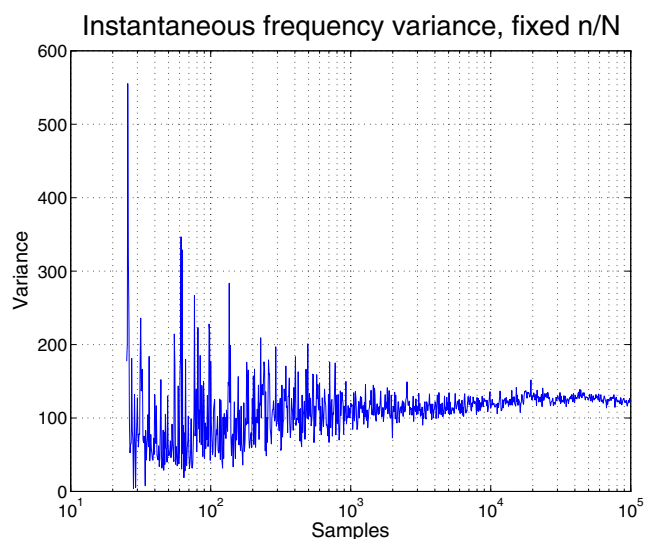
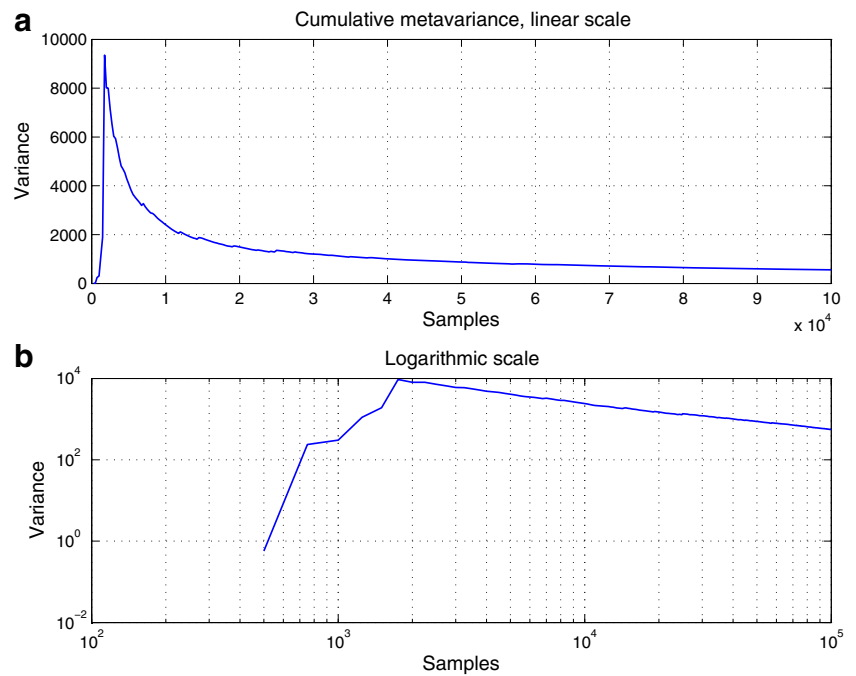


**Fig. 4** Pink (power law) noise with a power law exponent of  $\alpha=2$  was used as a surrogate signal. The number of phase resets per sample ( $n/N$ ) was held constant at 0.04 so as to observe the asymptotic behavior of  $f_v$  as the number of points in the signal increased. Results are plotted on a semi-logarithmic scale to emphasize that the  $f_v$  variance (“metavariance”) can be accurately captured from  $\sim 10^3$  samples

## Discussion

Our study had two principal aims: to establish a method for measuring metastable brain dynamics in children, and to use this new measure to study development in a cross-sectional cohort of young children of ages 2 – 6. Our method improves on other studies of brain metastability in development by (A) using frequency variance as a variable that corresponds to synchronization of cell assemblies, (B) showing applicability to minimal

**Fig. 5** Cumulative  $f_v$  variance (“metavariance”) for a surrogate pink noise signal with  $n/N=0.04$  averaged over 10 trials (a). Plotting in log-log coordinates (b) reveals a power law relationship (linear region) after  $N \approx 2 \times 10^3$ . This number is thus a useful estimate of the minimum data length necessary for meaningful measurement of  $f_v$



data with missing channels, and (C) avoiding measurements of phase relations between EEG sensors, which are not sensitive to global phase resets. Using surrogate signals with artificially induced phase resets, we showed that  $f_v$  is a good proxy for phase resetting. Having established the utility of the method, we showed that  $f_v$  correlates with age in young children and gives similar results with different lengths of recordings (Fig. 9), thus showing promise as a biomarker of typical and, by extension, atypical development.

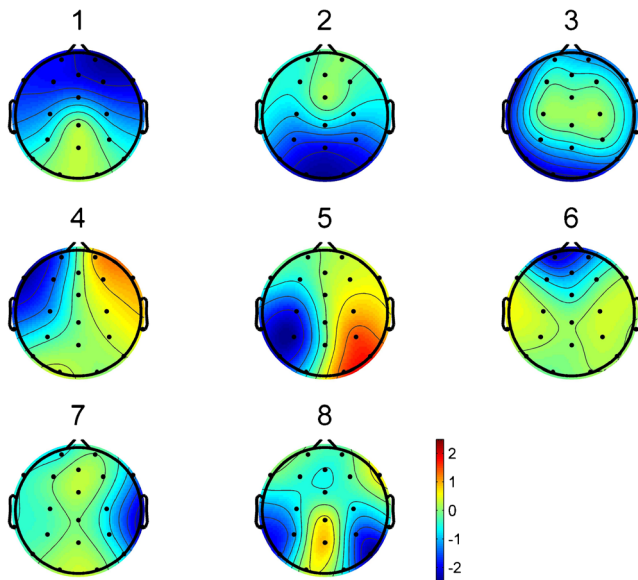


**Fig. 6** A combined PCA and ICA decomposition yielding 8 ICs. Only IC<sub>5</sub> features a strong, dipole-like scalp topography indicative of a brain-related component. Other ICs feature scalp topographies indicative of ocular artifacts (IC<sub>4</sub>, IC<sub>6</sub>), or were otherwise ambiguous in origin (IC<sub>1</sub>, IC<sub>2</sub>, IC<sub>3</sub>, IC<sub>7</sub>, IC<sub>8</sub>)

As stated previously, our new method for measuring frequency stability shows strong advantages for studying pediatric populations, in which children yield minimal data, over methods that directly measure the duration of metastable states, which are vulnerable to missing data. Our method allows noisy channels to be discarded with little consequence and can be applied to “virtual channels” such as brain-related ICs. Furthermore, our method takes into account the long range spatial correlations of phase resets, a consideration disregarded by a similar methodology practiced by Thatcher and colleagues (Thatcher et al. 2008, 2009a, b). Our method is also well suited for the short datasets often obtained from children, as it gives similar results with both maximal and truncated EEG recordings.

We demonstrated that  $f_v$  increases monotonically with noise as a function of the number of artificially induced phase resets in three surrogate signals: sinusoids, pink noise, and the logistic map (deterministic chaos) (Fig. 3). The relationship between  $f_v$  and the number of phase resets  $n$  is almost linear for small phase

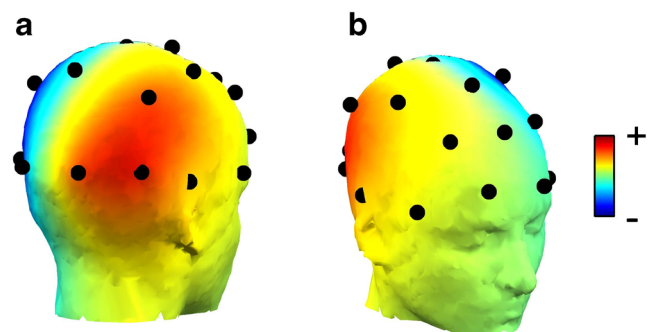


**Fig. 7** A left posterior IC was selected from the ICA decomposition as the focus for our analysis of frequency metastability and projected onto a sample head model

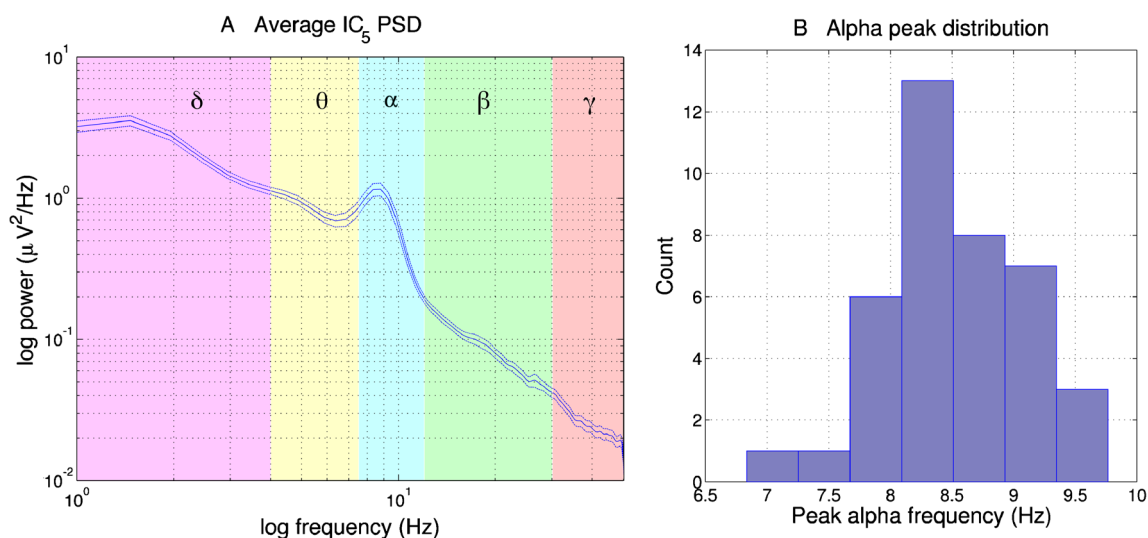


**Fig. 8** The PSD of each subject's IC<sub>5</sub> signal was computed via Welch's method, and the grand average of all PSDs plotted on a log-log scale (**a**), where *dotted lines* indicate standard error of the mean. Frequency bands are color coded for easy interpretation: delta (1–4 Hz; *purple*), theta (4–7.5 Hz; *yellow*), alpha (7.5–12 Hz; *blue*), beta (12–30 Hz; *green*), and gamma (30–50 Hz; *red*). The grand average PSD gave little indication of

muscle noise at beta or gamma frequencies, supporting our conclusion that data were sufficiently processed to remove muscle artifact. Furthermore, we observed that children had alpha rhythms within the traditional limits of the alpha bandpass, suggesting that phase resets also occurred within this frequency range. A histogram of peak alpha frequencies ( $8.6 \pm 0.67$  Hz) for all 39 subjects further supports this conclusion (**b**)

reset rate  $n/N$ , where  $N$  is length of data. For large  $n/N$ , the  $f_v(n)$  curve shows the relaxation characteristic of a hyperbolic tangent function with added noise. In a physiologically plausible scenario, an EEG signal with a sampling rate of 250 Hz and aperiodic alpha-frequency (10 Hz) phase resets (Freeman et al. 2003),  $n/N = 0.04$ , which is a sufficiently small ratio to approximate the  $f_v(n)$  curve as linear. For the fourth surrogate signal, Gaussian white noise,  $f_v$  did not increase as a function of  $n$ . Because the power spectrum of human EEG is power-law distributed (pink noise) rather than uniform (white noise) (Pritchard 1992), white noise is a poor model of EEG, and the finding that  $f_v$  does not increase with the number of artificially induced phase resets in white noise signals should not affect the validity of our subsequent analysis using empirical data better modeled as pink noise.

Having established that  $f_v$  is a good proxy for phase resetting in surrogate signals with similar properties to human EEG, we measured  $f_v$  while holding the rate of phase resets constant and increasing the length of surrogate data. The cumulative variance ("metavariance") was computed for the instantaneous frequency variance  $f_v$  averaged across signals from 10 simulated trials (Fig. 5). The curve follows a power law after  $N \approx 2 \times 10^3$  points, as evidenced by the linearization of the curve observed after applying the logarithmic transform. Power law relationships are scale-invariant and thus lack a time constant. The identification of a power law relationship between metavariance and the number of points in the simulated signal after  $N \approx 2 \times 10^3$  suggests that this is the minimum number of points needed to compute  $f_v$  with accuracy. Assuming that the minimal  $N$

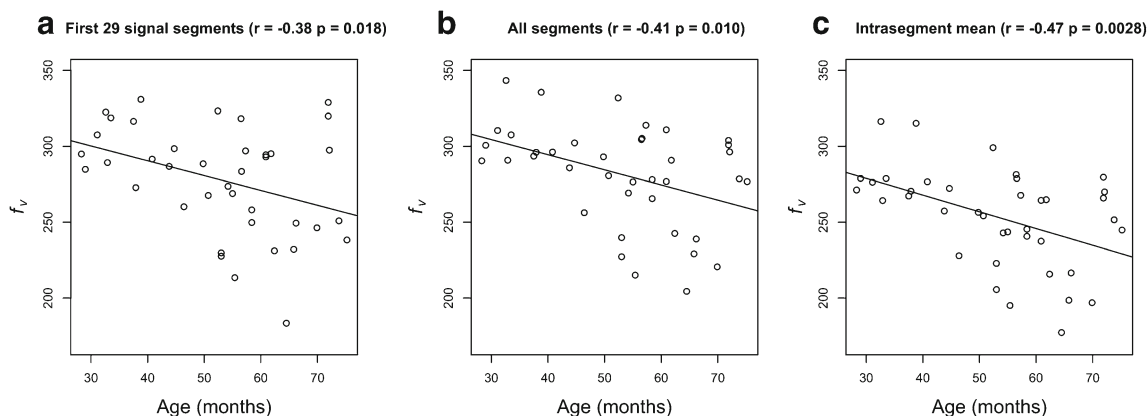


**Fig. 9** Three different correlation analyses of  $f_v$  and age were performed, one controlling for length of the IC signal (**a**), another using all clean segments of the IC signal (**b**), and a third using the intra-segment mean  $f_v$  of all segments from the IC of interest (**c**). Whereas the first two analyses

involved removing linear trends from signal segments, Analysis 3 did not. All three analyses found a significant negative correlation between age and  $f_v$ . However, Analysis 3 yielded the strongest correlation (see figure for  $r$  and  $p$  values)



necessary for accurate measurement of  $f_v$  depends on the number of phase resets in the recording, an inverse linear relationship between phase reset rate and minimum necessary recording length can be inferred. For instance, a signal with phase resets occurring at an average rate of 5 Hz would require  $N \approx 4 \times 10^3$ , i.e. twice the number of samples specified above. Even in the event that some children had slower average phase reset rates that simulated in our surrogate data, given a worst-case scenario in which phase resetting occurs at low theta rates, 6000 samples would be needed to obtain a signal with 80 phase resets. This is still shorter than our shortest clean signal, which contained ~7400 samples. We are therefore confident that all signals examined are sufficiently long for accurate measurement of  $f_v$ .

In the second half of our study, all 39 subjects had artifact-free EEG signals longer than the minimum signal length  $N = 2 \times 10^3$  established by the surrogate signal analysis ( $N = 2.19 \times 10^4 \pm 9.78 \times 10^3$ ;  $\min = 7.42 \times 10^3$ ,  $\max = 4.91 \times 10^4$ ). A left posterior brain-related IC was identified from the ICA decomposition of all subjects' EEG recordings (Figs. 6 and 7). Considering evidence that gamma signals recorded over posterior parietal regions are modulated by thalamic alpha activity (Roux et al. 2013), beta-gamma oscillations from this left posterior IC are strong candidates for phase reset carrier waves. This assertion is supported by two main points: phase resets are (A) known to occur at alpha rates in resting gamma signals (Freeman et al. 2003) and (B) thought to be timed and orchestrated by thalamic oscillations (Freeman et al. 2003; Thatcher et al. 2009b). Furthermore, unpublished data from our lab links left-posterior theta (4–7 Hz) power to level of functioning in young children with autism spectrum disorder (ASD). These facts, in conjunction with the observation that other ICs exhibited either ambiguous or artifact-related scalp topographies, justified our decision to select left posterior IC signals as targets for further analysis.

Inspection of the average PSD computed from this IC signal shows a spectral peak at 8–9 Hz, which is indicative of alpha rhythms (Fig. 8). Presuming that phase resets occur, on average, at alpha frequencies (Freeman et al. 2003), our model of 10 Hz phase resetting in surrogate signals closely matches the frequency of alpha oscillations in the children herein examined. Furthermore, the beta and gamma frequency bands of this averaged PSD show no spectral peaks indicative of electromyography (EMG) artifacts, supporting the conclusion that this IC signal is generated by brain-related activity.

Using signals from this IC, we were successful in correlating  $f_v$  with age in children ages 2–6, implying that frequency stability changes across early development. By applying the same methods while controlling for length of signal in Analysis 1 and using all artifact-free recordings in Analysis 2, we obtained virtually identical results, indicating that our method works well with the minimal-length signals often obtained from children. Taking the mean intra-segment  $f_v$  value for each subject without removing linear trends from individual segments (Analysis 3) yielded an even stronger correlation between age and  $f_v$  as

compared with the first two analyses (Fig. 9), both of which involved detrending the time courses of the segments. A likely reason for this finding is the fact that removing a linear trend from a signal decreases its variance, and is thus detrimental to measuring  $f_v$ . For signals with discontinuities created by concatenation, we believe the approach adopted in Analysis 3 is ideal for measuring  $f_v$ . Instantaneous frequency values for the left posterior IC examined in this study typically followed a leptokurtic distribution (Fig. 10), with values in the center of the distribution reflecting metastable frequency states and values in the small tails of the distribution reflecting phase resets (state transitions).

Contrary to our hypothesis, we found that  $f_v$  decreases with age, indicating that its inverse, frequency stability, increases with age. This result differs from the findings of prior studies which used different methods to measure brain variability. Two prior studies found that brain variability positively correlated with age in event related potentials (ERPs) of infants and children and negatively correlated with behavioral variability in reaction time and facial recognition (Lippé et al. 2009; McIntosh et al. 2008). Nonetheless, our findings can be interpreted by taking into account the fact that reciprocal connections between constituent neurons in cell assemblies are likely weak in early development, requiring several months to years of learning before synapses within the cell assembly are strongly potentiated. Long term potentiation (LTP) of cell assembly synapses increases the efficacy of

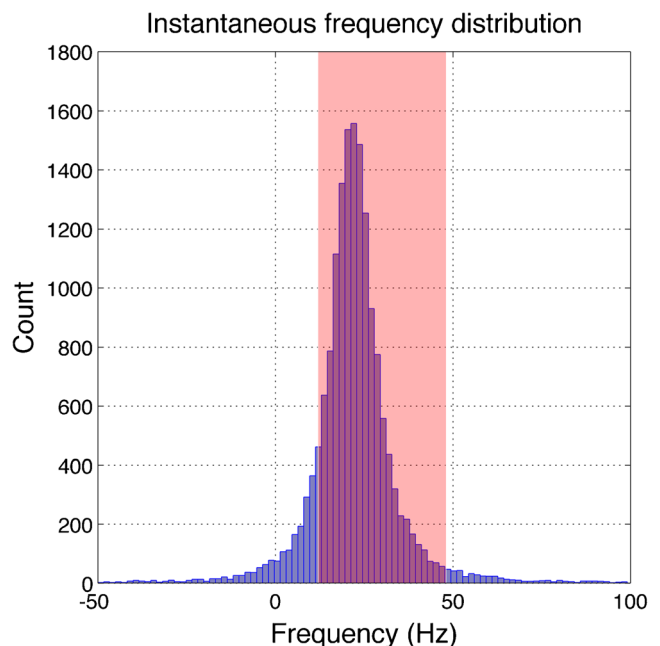


**Fig. 10** The instantaneous frequency  $f_v$  was computed from a typical dataset. Mean values were not subtracted from  $f_v$  values ( $\mu = 21.6$  Hz,  $\sigma = 15.2$  Hz) to obviate the leptokurtic distribution of values ( $N = 1.66 \times 10^4$ , kurtosis = 23.9) about the center of the 12–48 Hz frequency band. Frequencies within the frequency band are highlighted in red. Note that the mode of the distribution does not coincide with the center of the frequency band due to the presence of negative frequencies yielded by the Hilbert transform

constituent neurons to excite each other (Bliss and Collingridge 1993; Hughes 1958), resulting in a stronger, more stable assembly. Increased durations of stable synchrony within a cell assembly translate into lower frequency variance in the EEG signal.

Alternatively, it is possible that transitions between metastable frequency states do not reflect synchronization and desynchronization of cell assemblies and that our finding of correlation between frequency stability and age is serendipitous, yet not spurious. Prior work has postulated that phase resets result from inhibitory bursting in thalamocortical circuits (Freeman et al. 2003; Thatcher et al. 2009b). In particular, orchestration and timing of phase resets by the thalamus may help explain the astonishing spatiotemporal correlation of cortical phase resets. Phase resets in the resting-state EEG of healthy adults show strong spatial correlation over temporal intervals as brief as 5 ms, with phase velocities as large as 40 m/s, considerably faster than serial synaptic corticocortical conduction velocities (Freeman et al. 2003).

While a similar cross-sectional study of development used PCA to measure dimensionality as a metric of EEG signal variability (McIntosh et al. 2008), we did not use PCA for this purpose, nor did we make any direct estimates of state space dimensionality. However, the presence of chaotic transitions in recordings can nonetheless be used to infer a high-dimensional state space (Tsuda 2013). The dimensionality of a system betrays possible attractors thereof (closed subspaces of state space towards which trajectories evolve). For instance, systems with two or more dimensions are capable of periodic orbits (limit cycle attractors) and systems with three or more dimensions are capable of chaos (strange attractors, or extreme sensitivity to initial conditions). Metastability can be interpreted as saddle points in state space, which attract and repel trajectories in orthogonal directions, connected by heteroclinic channels (Fig. 11a). However, heteroclinic channels are unstable in low-dimensional systems. Alternatively, metastability may actually be chaotic itinerancy, the slowing of state space trajectories through quasi-attractors, or “ghosts” or recently destabilized attractors (Fig. 11b). Chaotic

itinerancy, like heteroclinic cycles, implies a high dimensional state space (Tsuda 2013). The inferred presence of transitory dynamics in our data thus suggests a high-dimensional system with the potential for exotic chaotic behavior (Letellier and Rössler 2007; Rössler 1979).

### Mechanisms of phase resetting

To gain deeper insight into the physical phenomenon of phase resetting, it is useful to consider phase resets in the context of nonlinear dynamics (Table 1). As stated earlier, phase resets are state transitions between metastable cortical frequency states. State transitions occur in dynamical systems when a control parameter is tuned past a critical value and a loss of stability occurs. A familiar example is the liquid to gas state transition which occurs when water is heated past its boiling point. In this context, temperature is a control parameter and the boiling point is a critical value. Might feedforward thalamocortical inhibition serve as a control parameter for phase resets? This is consistent with the observation that phase resets occur at alpha (7.5 – 12.5 Hz) rates in healthy adults (Freeman et al. 2003) and evidence suggesting that the phase of thalamic alpha activity modulates the power of cortical gamma signals (Roux et al. 2013), which are carrier waves for phase resets (Freeman et al. 2003). Bursts of gamma-aminobutyric acid (GABA)-mediated inhibition may attenuate the amplitude of the EEG signal, explaining previous findings of reduced signal amplitude coinciding with phase resets (Freeman et al. 2003). Such feedforward inhibition would disrupt bursts of synchronous firing in cortical pyramidal cells, which might subsequently transition to a new frequency of oscillations once disinhibited. Over the course of development, thalamocortical synapses onto inhibitory cortical interneurons may be lost during synaptic pruning (Bianchi et al. 2013; Huttenlocher 1979; Huttenlocher and Dabholkar 1997), explaining the increase in frequency stability with age observed in our recordings (Fig. 9). Over-pruning has already been hypothesized to trigger neurodevelopmental disorders such as schizophrenia (Feinberg 1982; Frohlich and van Horn

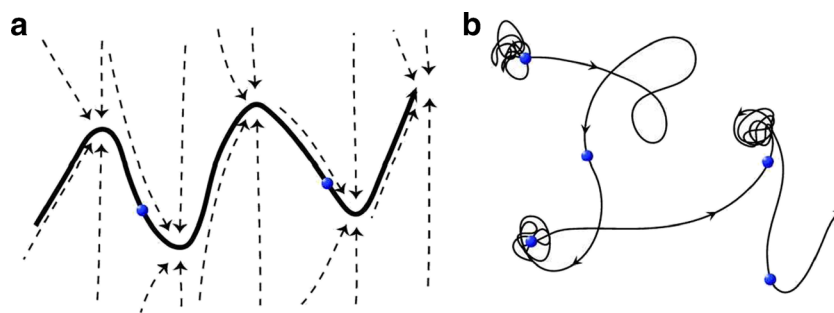


**Fig. 11** Possible scenarios for the mechanisms underlying metastability. Metastability may be the result of heteroclinic channels between metastable saddle points (a). Alternatively, the trajectory of the system

through state space may be interpreted as chaotic itinerancy (b), in which the trajectory is slowed by attractor ruins, or “ghosts” of recently destabilized attractors

**Table 1** Interpretations of frequency metastability

	Cell assembly synchronization	Inhibitory thalamocortical bursting
Computational model	Self-organized criticality (SOC)	Tuning-dependent state transition
Physical metaphor	Avalanche (sandpile model)	Thermodynamic phase transition (e.g., water boiling into steam)
Neural mechanism	Synchronization of neural networks	Gamma-aminobutyric acid (GABA) mediated feedforward inhibition
Cause of developmental changes	Synaptic potentiation between constituent neurons	Synaptic pruning weakening inhibitory afferents
Evidence	-Brain is far from equilibrium system  -Phase resets are aperiodic  -Neuronal avalanches reported in vitro -Critical state may enhance computational power of brain	-Explains anomalous phase velocities and spatiotemporal correlations of phase resets -Role of GABA <sub>A</sub> receptors in generating high frequency EEG rhythms -Possible relationship with thalamic alpha activity
Possible relevance to atypical development	-Cognitive inflexibility results from reduced ability of cell assemblies to form as neuronal avalanches	-GABA <sub>A</sub> receptor mutations associated with ASD: weakened thalamocortical inhibition

2014; Granger 1996; Kehler et al. 2008; Olney and Farber 1997), and may also explain differences in phase locking duration observed in ASD (Thatcher et al. 2009b), a disorder which is already associated with mutations in and abnormal expression levels of GABA<sub>A</sub> receptor genes (Fatemi et al. 2010, 2011; Kang and Barnes 2013; McCauley et al. 2004; Menold et al. 2001).

Although the timing and orchestration of phase resets might be explained in terms of subcortical mechanisms, the framework of nonlinear dynamics also allows for an explanation consistent with the theory that metastable states between phase resets represent the activation of cell assemblies. In nonequilibrium systems such as the brain, a critical point may serve as an attractor for the system, such that the system spontaneously undergoes state transitions without the tuning of a control parameter. This phenomenon, in which systems enjoy a wide repertoire of possible states by virtue of being poised near a critical point, is a hallmark of complexity known as self-organized criticality (SOC) (Bak et al. 1987, 1988). For example, one can imagine a sandpile which is built until its slope reaches a critical angle: adding additional sand to the pile will cause arbitrarily large avalanches ranging in size from a few grains of sand to a considerable portion of the pile. In this context, complexity cannot be explained in terms of the individual parts themselves, but rather in terms of feedback between a slow process (adding sand) which increases energy and a fast process (the avalanche) which dissipates energy. SOC is thus an attractive mechanism by which cell assemblies might spontaneously synchronize in the brain, with local synchrony propagating as a neuronal avalanche (Plenz and Thiagarajan 2007).

An important property of avalanches in SOC is scale-invariance or fractal organization (Bak et al. 1987). Scale invariance is observed at almost all levels of the brain,

generally in the form of pink noise, or  $1/f$  noise, where spectral power is inversely proportional to frequency (He 2014; Plenz and Thiagarajan 2007). Examples include the temporal distributions of ion channel openings (Toib et al. 1998), spike trains (Teich et al. 1997), neurotransmitter exocytosis (Lowen et al. 1997), and amplitude fluctuations (Linkenkaer-Hansen et al. 2001) as well as power spectral density (Pritchard 1992) in

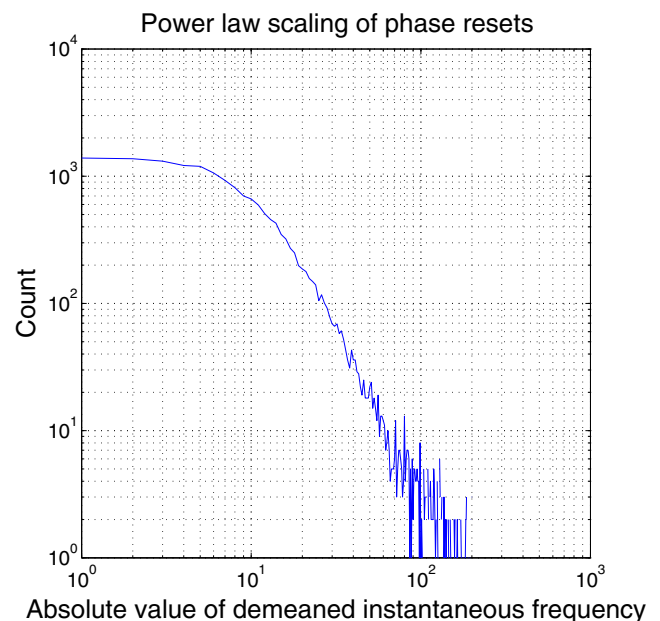


**Fig. 12** A linear region, indicative of power law scaling, is revealed by a log-log transform of the histogram of  $|f_v|$ . Power law relationships exist when one quantity varies as a power of the other. Such relationships are scale free, as scaling the first quantity by a constant factor only causes a proportional increase in the second quantity. Power laws and scale invariance are features of self-organized criticality (SOC), in which a system operating near a critical point experiences arbitrarily large fluctuations

EEG recordings. Spatially distributed brain data, such as the topology of functional brain networks, has also been shown to obey power laws (Sporns 2011). “Neuronal avalanches” have been widely reported in local field potential (LFP) recordings from in vitro cortical slices, taking the form of bursts of spatiotemporal activity following power law distributions (Beggs and Plenz 2003, 2004; Plenz and Thiagarajan 2007). In our study, the parameters of the empirical distribution associated with  $|f_v|$  revealed power law scaling in the limit of large  $|f_v|$ , as illustrated by a log-log transform (Fig. 12), suggesting that phase resets are, in fact, critical fluctuations driven by SOC in the brain. Regardless of the mechanism, this finding adds another entry to the vast body of work describing scale-invariance in the brain.

Two principal limitations of our study should be considered. Firstly, our study was performed cross-sectionally and therefore does not support the same firm conclusions one might draw from a longitudinal study. Additionally, in comparing our study to prior studies of metastability and brain variability in development (Koenig et al. 2002; Lippé et al. 2009; McIntosh et al. 2008; Thatcher et al. 2009a), we have simultaneously introduced a new method, a different age group, and, in some cases, a different paradigm. Not having controlled for all variables separately, reasons for differences between our findings and the findings of other groups remain uncertain.

Our recruitment of typically developing children was part of a larger study of atypical development, and our group is currently applying this method to age-matched children with ASD. Other future work should be focused along similar lines by examining changes in frequency stability with age in atypical development and neurodevelopmental disorders with onset in early childhood, such as ASD and attention deficit hyperactivity disorder (ADHD). Future studies should also use a longitudinal design to validate conclusions regarding the relationship between frequency stability and age.

**Acknowledgments** The authors are deeply grateful to all children and parents who volunteered their time to advance our knowledge of typical development. We thank Dr. Mikhail Rabinovich for his comments on theoretical aspects of this work, as well as Dr. Ted Hutman and Dr. Carrie Bearden for their much appreciated feedback on the manuscript. A warm thank you is also extended to Nima Chenari for his kind help producing illustrations and to Christina Shimizu, Andrew Sanders, and Amanda Noroña for their patience and professionalism in assisting with data collection. This work was supported by NIMH K23MH094517-01.

**Informed consent** All procedures followed were in accordance with the ethical standards of the responsible committee on human experimentation (institutional and national) and with the Helsinki Declaration of 1975, and the applicable revisions at the time of the investigation. Informed consent was obtained from all patients for being included in the study.

**Conflict of interest** Joel Frohlich, Andrei Irimia, and Shafali S. Jeste declare that they have no conflicts of interest.

## References

- Amari, S.-I., Cichocki, A., & Yang, H.H. (1996). A new learning algorithm for blind source separation. *Adv Neural Information Process Syst* 757–763.
- Bak, P., Tang, C., & Wiesenfeld, K. (1987). Self-organized criticality: an explanation of  $1/f$  noise. *Physical Review Letters*, 59, 381–384.
- Bak, P., Tang, C., & Wiesenfeld, K. (1988). Self-organized criticality. *Physical Review A*, 38, 364–374.
- Beggs, J. M., & Plenz, D. (2003). Neuronal avalanches in neocortical circuits. *The Journal of Neuroscience: The Official Journal of the Society for Neuroscience*, 23, 11167–11177.
- Beggs, J. M., & Plenz, D. (2004). Neuronal avalanches are diverse and precise activity patterns that are stable for many hours in cortical slice cultures. *The Journal of Neuroscience: The Official Journal of the Society for Neuroscience*, 24, 5216–5229.
- Bell, A. J., & Sejnowski, T. J. (1995). An information-maximization approach to blind separation and blind deconvolution. *Neural Computation*, 7, 1129–1159.
- Bianchi, S., Stimpson, C. D., Duka, T., Larsen, M. D., Janssen, W. G. M., Collins, Z., et al. (2013). Synaptogenesis and development of pyramidal neuron dendritic morphology in the chimpanzee neocortex resembles humans. *Proceedings of the National Academy of Sciences of the United States of America*, 110(Suppl 2), 10395–10401.
- Bliss, T. V., & Collingridge, G. L. (1993). A synaptic model of memory: long-term potentiation in the hippocampus. *Nature*, 361, 31–39.
- Bosl, W., Tierney, A., Tager-Flusberg, H., & Nelson, C. (2011). EEG complexity as a biomarker for autism spectrum disorder risk. *BMC Medicine*, 9, 18.
- Catarino, A., Churches, O., Baron-Cohen, S., Andrade, A., & Ring, H. (2011). Atypical EEG complexity in autism spectrum conditions: a multiscale entropy analysis. *Clinical Neurophysiology: Official Journal of the International Federation of Clinical Neurophysiology*, 122, 2375–2383.
- Coffey, D. S. (1998). Self-organization, complexity and chaos: the new biology for medicine. *Nature Medicine*, 4, 882–885.
- Cox, A., Klein, K., Charman, T., Baird, G., Baron-Cohen, S., Swettenham, J., et al. (1999). Autism spectrum disorders at 20 and 42 months of age: stability of clinical and ADI-R diagnosis. *Journal of Child Psychology and Psychiatry*, 40, 719–732.
- Luca C De, Leventer, R. (2010). Developmental trajectories of executive functions across the lifespan. *Exec Funct Front Lobes Lifesp Perspect* 23–56.
- Delorme, A., & Makeig, S. (2004). EEGLAB: an open source toolbox for analysis of single-trial EEG dynamics including independent component analysis. *Journal of Neuroscience Methods*, 134, 9–21.
- Eldridge, J., Lane, A. E., Belkin, M., & Dennis, S. (2014). Robust features for the automatic identification of autism spectrum disorder in children. *Journal of Neurodevelopmental Disorders*, 6, 12.
- Elliot, C. D. (2007). *Differential ability scales* (2nd ed.). San Antonio: Harcourt Assessment.
- Fatemi, S. H., Reutiman, T. J., Folsom, T. D., Rooney, R. J., Patel, D. H., & Thuras, P. D. (2010). mRNA and protein levels for GABAA $\alpha$ 4,  $\alpha$ 5,  $\beta$ 1 and GABABR1 receptors are altered in brains from subjects with autism. *Journal of Autism and Developmental Disorders*, 40, 743–750.
- Fatemi, S. H., Folsom, T. D., Kneeland, R. E., & Liesch, S. B. (2011). Metabotropic glutamate receptor 5 upregulation in children with autism is associated with underexpression of both Fragile X mental retardation protein and GABAA receptor  $\beta$ 3 in adults with autism. *Anatomical Record Hoboken NJ* 2007, 294, 1635–1645.
- Feinberg, I. (1982). Schizophrenia: caused by a fault in programmed synaptic elimination during adolescence? *Journal of Psychiatric Research*, 17, 319–334.



- Fell, J., Rösche, J., & Beckmann, P. (1993). Deterministic chaos and the first positive Lyapunov exponent: a nonlinear analysis of the human electroencephalogram during sleep. *Biological Cybernetics*, 69, 139–146.
- Fountain, C., King, M. D., & Bearman, P. S. (2011). Age of diagnosis for autism: individual and community factors across 10 birth cohorts. *Journal of Epidemiology and Community Health*, 65, 503–510.
- Freeman, W. J. (2003). Evidence from human scalp electroencephalograms of global chaotic itinerancy. *Chaos Woodbury N*, 13, 1067–1077.
- Freeman, W. J. (2004a). Origin, structure, and role of background EEG activity. Part 1. Analytic amplitude. *Clinical Neurophysiology: Official Journal of the International Federation of Clinical Neurophysiology*, 115, 2077–2088.
- Freeman WJ (2004b). Origin, Structure, and Role of Background EEG Activity. Part 2: Analytic Phase. *Clin Neurophysiol* 2089–2107.
- Freeman, W. J., & Holmes, M. D. (2005). Metastability, instability, and state transition in neocortex. *Neural Network: the Official Journal of the International Neural Network Society*, 18, 497–504.
- Freeman, W. J., & Kozma, R. (2010). Freeman's mass action. *Scholarpedia*, 5, 8040.
- Freeman, W. J., Burke, B. C., & Holmes, M. D. (2003). Aperiodic phase re-setting in scalp EEG of beta-gamma oscillations by state transitions at alpha-theta rates. *Human Brain Mapping*, 19, 248–272.
- Freeman, W. J., Holmes, M. D., West, G. A., & Vanhatalo, S. (2006). Fine spatiotemporal structure of phase in human intracranial EEG. *Clinical Neurophysiology: Official Journal of the International Federation of Clinical Neurophysiology*, 117, 1228–1243.
- Friston, K. J. (1996). Theoretical neurobiology and schizophrenia. *British Medical Bulletin*, 52, 644–655.
- Friston, K. J. (2000). The labile brain. I. Neuronal transients and nonlinear coupling. *Philosophical Transactions of the Royal Society of London. Series B: Biological Sciences*, 355, 215–236.
- Frohlich, J., & van Horn, J. D. (2014). Reviewing the ketamine model for schizophrenia. *Journal of Psychopharmacology Oxford England*, 28, 287–302.
- Ghanbari, Y., Bloy, L., Christopher Edgar, J., Blaskey, L., Verma, R., & Roberts, T. P. L. (2013). Joint analysis of band-specific functional connectivity and signal complexity in autism. *Journal of Autism and Developmental Disorders*. doi:10.1007/s10803-013-1915-7.
- Granger, B. (1996). [Synaptogenesis and synaptic pruning: role in triggering schizophrenia]. *Presse Médicale Paris France* 1983, 25, 1595–1598.
- He, B. J. (2014). Scale-free brain activity: past, present, and future. *Trends in Cognitive Science*. doi:10.1016/j.tics.2014.04.003.
- Hebb, D. (1949). *The organization of behavior: A neuropsychological theory*. New York: Wiley.
- Hertz-Picciotto, I., & Delwiche, L. (2009). The rise in autism and the role of age at diagnosis. *Epidemiology (Cambridge, Mass)*, 20, 84–90.
- Hofstadter, D. (1979). *Gödel, Escher, Bach: An eternal golden braid*. New York: Basic Books.
- Hughes, J. R. (1958). Post-tetanic potentiation. *Physiological Reviews*, 38, 91–113.
- Huttenlocher, P. R. (1979). Synaptic density in human frontal cortex - developmental changes and effects of aging. *Brain Research*, 163, 195–205.
- Huttenlocher, P. R., & Dabholkar, A. S. (1997). Regional differences in synaptogenesis in human cerebral cortex. *Journal of Comparative Neurology*, 387, 167–178.
- Janjarsjitt, S., Scher, M. S., & Loparo, K. A. (2008). Nonlinear dynamical analysis of the neonatal EEG time series: the relationship between neurodevelopment and complexity. *Clinical Neurophysiology: Official Journal of the International Federation of Clinical Neurophysiology*, 119, 822–836.
- Kang, J.-Q., & Barnes, G. (2013). A common susceptibility factor of both autism and epilepsy: functional deficiency of GABA A receptors. *Journal of Autism and Developmental Disorders*, 43, 68–79.
- Kaplan, T., Fingelkurts, A., Fingelkurts, A., Borisov, S. V., & Darkhovsky, B. (2005). Nonstationary nature of the brain activity as revealed by EEG/MEG: methodological, practical and conceptual challenges. *Signal Processing*, 85, 2190–2212.
- Kehrer, C., Maziashvili, N., Dugladze, T., & Gloveli, T. (2008). Altered excitatory-inhibitory balance in the NMDA-hypofunction model of schizophrenia. *Frontiers in Molecular Neuroscience*, 1, 6.
- Koenig, T., Prichep, L., Lehmann, D., Sosa, P. V., Braeker, E., Kleinlogel, H., et al. (2002). Millisecond by millisecond, year by year: normative EEG microstates and developmental stages. *NeuroImage*, 16, 41–48.
- Lee, T. W., Girolami, M., & Sejnowski, T. J. (1999). Independent component analysis using an extended infomax algorithm for mixed subgaussian and supergaussian sources. *Neural Computation*, 11, 417–441.
- Letellier, C., & Rössler, O. (2007). Hyperchaos. *Scholarpedia*, 2, 1936.
- Linkenkaer-Hansen, K., Nikouline, V. V., Palva, J. M., & Ilmoniemi, R. J. (2001). Long-range temporal correlations and scaling behavior in human brain oscillations. *The Journal of Neuroscience: The Official Journal of the Society for Neuroscience*, 21, 1370–1377.
- Lippé, S., Kovacevic, N., & McIntosh, A. R. (2009). Differential maturation of brain signal complexity in the human auditory and visual system. *Frontiers in Human Neuroscience*, 3, 48.
- Little, M. A., McSharry, P. E., Roberts, S. J., Costello, D. A. E., & Moroz, I. M. (2007). Exploiting nonlinear recurrence and fractal scaling properties for voice disorder detection. *Biomedical Engineering Online*, 6, 23.
- Lowen, S. B., Cash, S. S., Poo, M., & Teich, M. C. (1997). Quantal neurotransmitter secretion rate exhibits fractal behavior. *The Journal of Neuroscience: The Official Journal of the Society for Neuroscience*, 17, 5666–5677.
- Manor, B., & Lipsitz, L. A. (2012). Physiologic complexity and aging: implications for physical function and rehabilitation. *Progress in Neuropsychopharmacology and Biological Psychiatry*. doi:10.1016/j.pnpbp.2012.08.020.
- McCauley, J. L., Olson, L. M., Delahanty, R., Amin, T., Nurmi, E. L., Organ, E. L., et al. (2004). A linkage disequilibrium map of the 1-Mb 15q12 GABA(A) receptor subunit cluster and association to autism. *American Journal of Medical Genetics. Part B, Neuropsychiatric Genetics: the Official Publication of the International Society of Psychiatric Genetics*, 131B, 51–59.
- McIntosh, A. R., Kovacevic, N., & Itier, R. J. (2008). Increased brain signal variability accompanies lower behavioral variability in development. *PLoS Computational Biology*, 4, e1000106.
- Menold, M. M., Shao, Y., Wolpert, C. M., Donnelly, S. L., Raiford, K. L., Martin, E. R., et al. (2001). Association analysis of chromosome 15 GABA<sub>A</sub> receptor subunit genes in autistic disorder. *Journal of Neurogenetics*, 15, 245–259.
- Meyer-Lindenberg, A. (1996). The evolution of complexity in human brain development: an EEG study. *Electroencephalography and Clinical Neurophysiology*, 99, 405–411.
- Mullen, E. M. (1995). *Mullen scales of early learning: AGS edition*. Circle Pines, MN: American Guidance Service.
- Olney, J. W., & Farber, N. B. (1997). Discussion of Bogerts' temporolimbic system theory of paranoid schizophrenia. *Schizophrenia Bulletin*, 23, 533–536.
- Onton, J., Westerfield, M., Townsend, J., & Makeig, S. (2006). Imaging human EEG dynamics using independent component analysis. *Neuroscience and Biobehavioral Reviews*, 30, 808–822.
- Philips, B. (2009). CircStat: a MATLAB toolbox for circular statistics. *Journal of Statistical Software*, 31, 1–21.
- Plenz, D., & Thiagarajan, T. C. (2007). The organizing principles of neuronal avalanches: cell assemblies in the cortex? *Trends in Neurosciences*, 30, 101–110.
- Pritchard, W. S. (1992). The brain in fractal time: 1/f-like power spectrum scaling of the human electroencephalogram. *International Journal of Neuroscience*, 66, 119–129.



- Rabinovich, M. I., Huerta, R., Varona, P., & Afraimovich, V. S. (2008). Transient cognitive dynamics, metastability, and decision making. *PLoS Computational Biology*, 4, e1000072.
- Rössler, O. (1979). An equation for hyperchaos. *Physics Letters A*, 71, 155–157.
- Roux, F., Wibrat, M., Singer, W., Aru, J., & Uhlhaas, P. J. (2013). The phase of thalamic alpha activity modulates cortical gamma-band activity: evidence from resting-state MEG recordings. *The Journal of Neuroscience: The Official Journal of the Society for Neuroscience*, 33, 17827–17835.
- Soong, A. C., & Stuart, C. I. (1989). Evidence of chaotic dynamics underlying the human alpha-rhythm electroencephalogram. *Biological Cybernetics*, 62, 55–62.
- Sporns, O. (2011). *Networks of the brain*. Cambridge, MA: MIT Press.
- Stam, C. J. (2005). Nonlinear dynamical analysis of EEG and MEG: review of an emerging field. *Clinical Neurophysiology: Official Journal of the International Federation of Clinical Neurophysiology*, 116, 2266–2301.
- Teich, M. C., Heneghan, C., Lowen, S. B., Ozaki, T., & Kaplan, E. (1997). Fractal character of the neural spike train in the visual system of the cat. *Journal of the Optical Society of America. A, Optics, Image Science, and Vision*, 14, 529–546.
- Thatcher, R. W., North, D. M., & Biver, C. J. (2008). Intelligence and EEG phase reset: a two compartmental model of phase shift and lock. *NeuroImage*, 42, 1639–1653.
- Thatcher, R. W., North, D. M., & Biver, C. J. (2009a). Self-organized criticality and the development of EEG phase reset. *Human Brain Mapping*, 30, 553–574.
- Thatcher, R. W., North, D. M., Neubrander, J., Biver, C. J., Cutler, S., & Defina, P. (2009b). Autism and EEG phase reset: deficient GABA mediated inhibition in thalamo-cortical circuits. *Developmental Neuropsychology*, 34, 780–800.
- Toib, A., Lyakhov, V., & Marom, S. (1998). Interaction between duration of activity and time course of recovery from slow inactivation in mammalian brain Na<sup>+</sup> channels. *The Journal of Neuroscience: The Official Journal of the Society for Neuroscience*, 18, 1893–1903.
- Tononi, G., & Edelman, G. M. (1998). Consciousness and complexity. *Science*, 282, 1846–1851.
- Tsuda, I. (2013). Chaotic itinerancy. *Scholarpedia*, 8, 4459.
- Varela, F. J. (1995). Resonant cell assemblies: a new approach to cognitive functions and neuronal synchrony. *Biological Research*, 28, 81–95.
- Wang, X., Meng, J., Tan, G., & Zou, L. (2010). Research on the relation of EEG signal chaos characteristics with high-level intelligence activity of human brain. *Nonlinear Biomedical Physics*, 4, 2.
- Werner, G. (2007). Metastability, criticality and phase transitions in brain and its models. *Biosystems*, 90, 496–508.